Hindawi
Advances in Materials Science and Engineering
Volume 2020, Article ID 8340685, 8 pages
https://doi.org/10.1155/2020/8340685

Research Article

Influence of 3D Printed Topological Structure on Lightweight Mullite Load Bearing Board in Thermal Environment

Yiran Man,[1] Xudong Luo ,[1] Zhipeng Xie,[2] and Dianli Qu [1]

[1]*School of Materials and Metallurgy, University of Science and Technology, Liaoning, Anshan 114051, China*
[2]*State Key Lab of New Ceramics and Fine Processing, School of Materials Science and Engineering, Tsinghua University, Beijing 100024, China*

Correspondence should be addressed to Xudong Luo; luoxudongs@aliyun.com

Received 18 January 2020; Revised 11 February 2020; Accepted 14 February 2020; Published 11 March 2020

Guest Editor: Shengli Jin

Copyright © 2020 Yiran Man et al. This is an open access article distributed under the Creative Commons Attribution License, which permits unrestricted use, distribution, and reproduction in any medium, provided the original work is properly cited.

In order to achieve the purpose of resource and energy saving in the process of producing ceramics products, the hollow lightweight load bearing board in thermal environment with topological structures was made by 3D printing. In this study, the load bearing board manufactured with different topological structures such as vertical grid, oblique square grid, and honeycomb grid was printed by direct ink writing technology using the same raw material of kaolin clay and α-Al_2O_3 powder. The three kinds of samples were sintered at 1450°C × 3 h. The effect of printed structures on mechanical property of load bearing board samples was investigated. Moreover, the finite element simulation was used to study the stress distribution of the load bearing board. Comparing with results obtained by three kinds of samples, honeycomb grid supported samples proved to be the most appropriate structure in various directions comprehensively.

1. Introduction

Lightweight structures enable a required technical functionality at lower weight than those generally achievable by other ways. Lightweight structures can be implemented by using less material or by providing more functionality or improved functionality through lighter structures. Cost of operation can also be reduced by using lighter products [1]. The load bearing board is a common solid plate structure accessory in the field of ceramic industry. In the process of ceramic production, the green parts of ceramic products are placed on the boards, and then the boards are moved into the kiln for sintering. Lightweight load bearing board plays an important role in saving energy and reducing resource consumption and also makes a significant contribution to environmental protection. Lightweight load bearing board can be achieved in two aspects: using lightweight materials or adopting a lighter structure. Thereinto, research relating to lightweight materials has been widely investigated. With α-Al_2O_3 as raw material and corn starch as pore forming agent, light alumina with low bulk density, low apparent porosity, and high closed porosity can be obtained by adjusting process parameters [2]. Lightweight Al_2O_3-$MgAl_2O_4$ refractory was obtained through the carbothermal reduction of MgO, the oxygen diffusion rate controlled oxidation of Mg vapor, and subsequent reaction between MgO and Al_2O_3 [3]. What is more, lightweight clay bricks which can be used as construction bricks or used in thermal/sound insulation used corn cob as pore forming agent and obtained flexural strength of 3–6 MPa [4]. However, the research on the lightweight structures of the load bearing board is not reported. To achieve lightweight products, it should consider not only lightweight materials, but also lighter structures.

The development of 3D printing technology provides conditions for the study of lightweight structures of the load bearing board. 3D printing is an additive manufacturing process used to build three-dimensional structures from computer aided design (CAD) models [5]. 3D printing is a unique manufacturing approach enabling the flexible preparation of highly complex and precise structures which are often difficult to be realised using traditional fabrication

methods such as casting and machining. With the development of 3D printing technology, more complex structures can be produced by 3D printing [6]. Eckel et al. studied the structures by fabricating microlattice and honeycomb structures with polymer-derived ceramics using SLA 3D printing technology and the structures obtained compressive strength as high as 163.3 MPa [7]. 3D Inkjet printing technology was adopted to manufacture scalable milli-scale reactors with porous structure [8]. Biranchi et al. studied the effects of the design parameters on the mechanical property of honeycomb cellular structures printed by fused deposition modelling (FDM) process. In order to obtain higher strength and elastic modulus of honeycomb structure, the honeycomb size should be kept below 4 mm, and the wall thickness should be kept around 3 mm [9]. Research of Tomislav et al. determined the effect of sample's structure on the tensile strength of 3D printed samples with Inkjet printing and revealed that the sample having the highest strength is honeycomb structure [10]. However, the above works have not been studied in the relationship between 3D printing structure of load bearing board and mechanical property systematically.

Taking its availability, printing speed, accuracy of printed parts, and functional cost [11] into account, DIW (direct ink writing) 3D printing technology is the most appropriate for the manufacture of load bearing board. In order to realize lightweight structure of load bearing board, samples of load bearing board supported with different topological structures such as vertical grid, oblique square grid, and honeycomb grid were printed by DIW 3D printing technology to replace the completely solid load bearing board using kaolin as raw material. The oblique square grid was designed by reference to the truss lattice structure. The truss lattice structure and the honeycomb structure were extensively applied in engineering due to low density and cost as well as high stiffness/strength characteristics [12, 13]. And the vertical structure, as a primary hollow structure, was designed as a control group. During the process of 3D printing, almost the same weight of slurry was used for each structure. The effects of different structures on mechanical and thermal property of load bearing board were studied. Moreover, the finite element simulation was used to study the damage mechanism of the load bearing boards.

2. Experiment

2.1. Raw Material and Green Body Preparation. The raw materials used in this experiment were kaolin clay and commercial Al_2O_3 powder with a purity of 99.9% and an average particle size of 80 μm. Chemical composition of kaolin clay is listed in Table 1. The mass ratio of dried kaolin clay and Al_2O_3 powder was 1 : 1.7 in the mixed powers. In this case, the mole ratio of $Al_2O_3 : SiO_2$ was slightly higher than 3 : 2 [14]. The mixed powders were ball-milled, dried, and then mixed with 20 wt.% water by a vacuum pug mill. The viscosity of the mixed slurry was about 12,000 mPa·s and it exhibited adequate plasticity for DIW 3D printing technology process.

Table 1: Chemical composition of raw materials.

Raw materials	SiO_2	CaO	Fe_2O_3	Al_2O_3	MgO	Na_2O
Kaolin	72.87	0.10	0.32	16.23	0.92	6.19

SolidWorks software was used to create 3D models of three different types of structures of load bearing board. Three types of structures are shown in Figure 1. Most of the load bearing board is solid plate structure, and sizes of the load bearing board are 300 mm × 300 mm × 30 mm, 100 mm × 100 mm × 25 mm, 50 mm × 50 mm × 20 mm, and so on. Dimension of a sample was set as 80 mm (length) × 20 mm (width) × 80 mm (height) according to the conditions of the equipment. Then the parameters of 3D printer (SYNO—SOURCE) were set by Simplify3D software: the diameter of the needle was 1 mm, the height of the layer was 0.7 mm, and the printing speed was 3000 mm/min, with no support and no heating, and consumption of slurry was almost the same. Afterwards the 3D printer printed the green body of load bearing board samples layer by layer according to the preset parameters. Printed samples are shown in Figure 2.

2.2. Postprocessing of Green Body. The green body was printed by DIW technology, so residual water in green body needed to be released. In this work, a dryer (JC101) was adopted to remove residual water. The dryer was set to 120°C × 8 h. The weight of dried three kinds of green bodies was 187.17 g, 189.62 g, and 188.34 g, respectively.

Green bodies were sintered at 1450°C × 3 h by a high-temperature furnace (SX18-4-5YM, China).

2.3. Sample Characterization. Thermal decomposition behavior was evaluated by thermogravimetric analysis (TGA) (TGA, HCT-4, China). The phase composition of sintered load bearing board samples with different structures was characterized by XRD (Philips X' pert-MPD, Holland). And the microstructure was examined on a field emission scanning electron microscope (Zeiss∑IGMAHD, Germany). In order to show the mechanical anisotropy of the samples, the cold modulus of rupture was adopted to characterize the strength of the samples. The cold modulus of rupture of samples in the perpendicular and parallel direction of layers was tested by testing apparatus (DPK-500N, China), respectively. The cold modulus of rupture was calculated by three-point bending according to the following formula:

$$\sigma_f = \frac{3PL}{2bh^2}, \quad (1)$$

where P is load at fracture (N), L is the span (mm), b is the width of the sample (mm), and h is the height of the sample (mm). It was worth mentioning that, in order to exhibit the differences in strength between 3D printed hollow load bearing board and ordinary solid load bearing board, the volumes of three kinds of hollow samples were considered to be the volume of enclosed space occupied by hollow samples. So b and h in this were valued as the total width/height of the

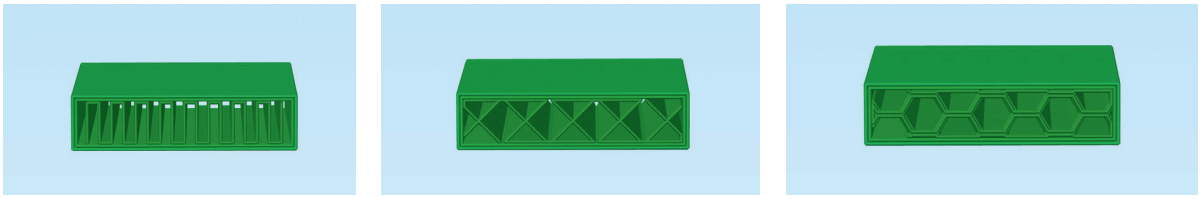

(a) (b) (c)

Figure 1: 3D models of different structures of load bearing board: (a) vertical supporting structure, (b) oblique square grid supporting structure, and (c) honeycomb grid supporting structure.

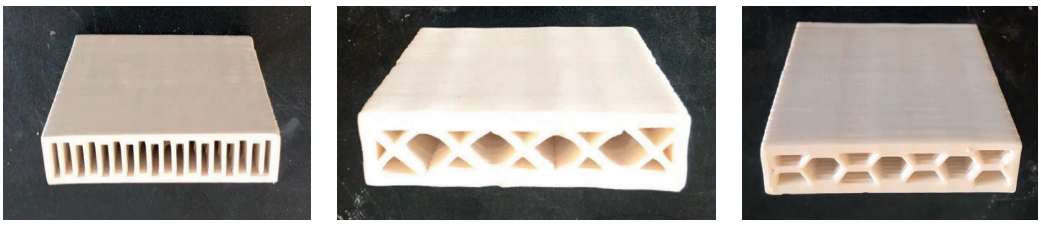

(a) (b) (c)

Figure 2: Printed green bodies: (a) vertical supporting structure, (b) oblique square grid supporting structure, and (c) honeycomb grid supporting structure.

samples placed on the testing apparatus. The loading rate was 0.05 mm/min; the span was 40 mm.

2.4. Finite Element Model. Finite element models were established by Abaqus CAE with more than 7000 nodes and 4000 C3D8R units in order to simulate the stress distribution in the bending strength test. The element size was about 1 mm × 1 mm × 1 mm. Material was defined by two mechanical properties: Young's modulus, $E = 30$ GPa, and Poisson's ratio, $\nu = 0.15$. Young's modulus and Poisson's ratio referred to the range given by Hsiung's research [15]. Boundary conditions correspond to bending strength testing conditions where all the nodes at midline of the top surfaces were subject to a constant load and the span of 40 mm was set at the bottom surface of model.

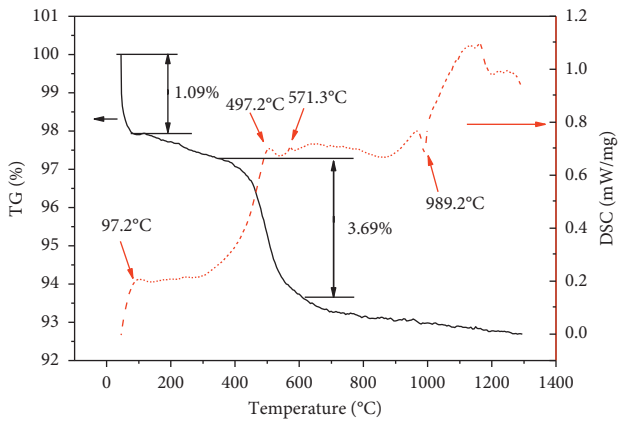

Figure 3: Thermal decomposition behavior of the slurry.

3. Results and Discussion

3.1. Thermal Decomposition and Sintering of the Green Parts. The mullite ceramic raw materials used in DIW 3D printing technology were analyzed by TG-DSC at a heating rate of 10°C/min, as shown in Figure 3. The TG-DSC curve was obtained for slurry used for printing. There were three endothermic peaks at 97.2°C, 497.2°C, and 571.3°C and one exothermic peak at 989.2°C in Figure 3, respectively. Around the peak at 97.2°C, about 1.09% of mass loss was produced at the first stage from the room temperature to 200°C because the physically adsorbed water was removed from the sample; around the peak at 497.2°C, a contribution to 3.69% of mass loss was caused by the kaolinite mineral dehydroxylation, forming metakaolin, which consists of the kaolinite lattice after the removal of most of the hydroxyl groups [16]. The α to β phase transition of quartz in the raw materials occurred at the temperature of 571.3°C [17]. Mullite began to form around the temperature of 989.2°C.

The sintering process was designed considering the TGA results. The heating rate was kept at 10°C/min when the temperature was from room temperature to 400°C. Then the heating rate slowed down to 5°C/min when the temperature was between 400°C and 600°C to make the kaolinite mineral dehydroxylation and quartz transform from α to β phase completely. After that, the heating rate was kept as 10°C/min until 1000°C and the temperature was kept constant for 3 h. Finally, the green bodies were sintered at 1450 × 3 h. Then cooling rate was set as 5°C/min when the temperature was higher than 500°C and natural furnace cooling was adopted when the temperature was below 500°C. The temperature curves used for the sintering process are shown in Figure 4.

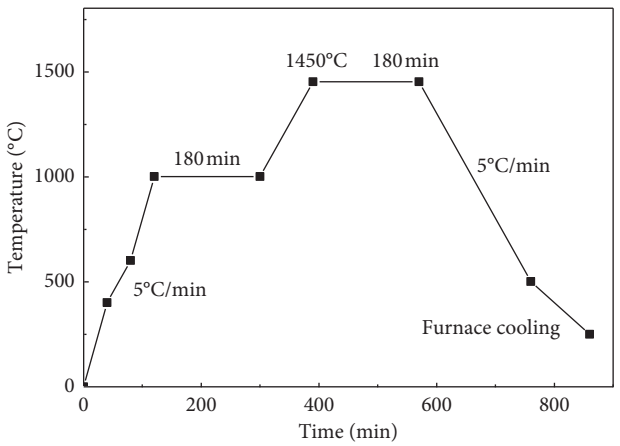

Figure 4: Sintering schedule of the samples.

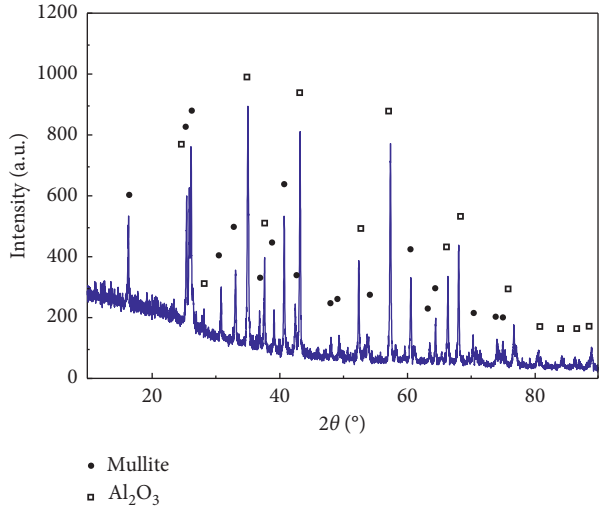

Figure 5: XRD patterns of sintered sample.

3.2. Phase Analysis. The XRD spectrums of sintered sample are shown in Figure 5. As can been seen, the new phase of calcined samples was mullite. Because of its excellent properties such as low thermal conductivity, good chemical stability, high-temperature creep resistance, and high surface area [18], load bearing board with mullite phase could have excellent property. The other phase of calcined samples was Al_2O_3. It indicated that the Silicate in the sample was consumed.

3.3. Performance. Cold modulus of rupture of the load bearing board supported with various structures was tested perpendicular to the layers and parallel to the layers, respectively (as shown in Figure 6).

As illustrated in Figure 6, when the load was perpendicular to the layers, samples with vertical supporting structure exhibited the lowest cold modulus of rupture and samples with honeycomb grid supporting structure exhibited the highest one. Slurry lines extruded by the 3D printer in the internal structure of sample with various structures were relatively isolated, and the internal support was only sintered and connected with the shell depending on the moving trail of 3D printer. When the sample was loaded along the vertical direction, the load was concentrated in a small area, which caused the specimen to fracture vertically at the loading place (shown in Figures 7(a) and 7(d)). Slurry lines in the internal structure of sample with oblique square grid structures were connected by points contact. When the specimen was subjected to load along the perpendicular direction, the internal grid structure can disperse the load in a larger area. When the specimen broke, larger load was required (shown in Figures 7(b) and 7(e)). Slurry lines in the internal structure of sample with honeycomb grid structures were connected by lines contact. It made the internal structure more integral and stronger (shown in Figures 7(c) and 7(f)).

In parallel direction, samples with vertical supported structure exhibited the highest cold modulus of rupture and samples with oblique square grid supported structure exhibited the lowest one. When the load was applied parallel to the layers, the angles between internal structure of three types samples (vertical grid, oblique square grid, and honeycomb grid) and the load were 0°, 45°, and 30°, respectively. An increase in loading angle decreased the cold modulus of rupture of the load bearing board supported with various structures [19].

Among three types of structures, samples with vertical supported structure exhibited the highest cold modulus of rupture in perpendicular and minimum cold modulus of rupture in parallel. The anisotropy in 3D printed products was displayed sufficiently. Comparing with results obtained by three kinds of samples, honeycomb grid supported samples proved to be the most appropriate structure in various directions comprehensively.

3.4. Simulation. The stress components at integration points of three kinds of samples in perpendicular and parallel direction of finite element are shown in Figure 8. The tensile/compressive trend under the load of three kinds of samples is shown in Figure 9. It could be easily concluded that under the perpendicular load distribution stress in the sample with vertical supporting structure was more nonuniform and the stress concentration was more evident. By contrast, sample with honeycomb grid supporting structure exhibited a stable situation. That may be the reason that sample with honeycomb grid supporting structure exhibited the highest cold modulus of rupture in perpendicular direction in the three-point bending test.

When the load was loaded in parallel direction, it could be easily seen that there was one green band on the top surface of sample (as shown in Figures 8(d)–8(f)). Green band was continuously distributed on the top surface in Figure 8(d). It can be inferred that inner structure made the stress dispersed in every column and there were more columns in structure with vertical supporting so that the stress distribution of the vertical supporting structure sample was more uniform than the other two kinds of structures.

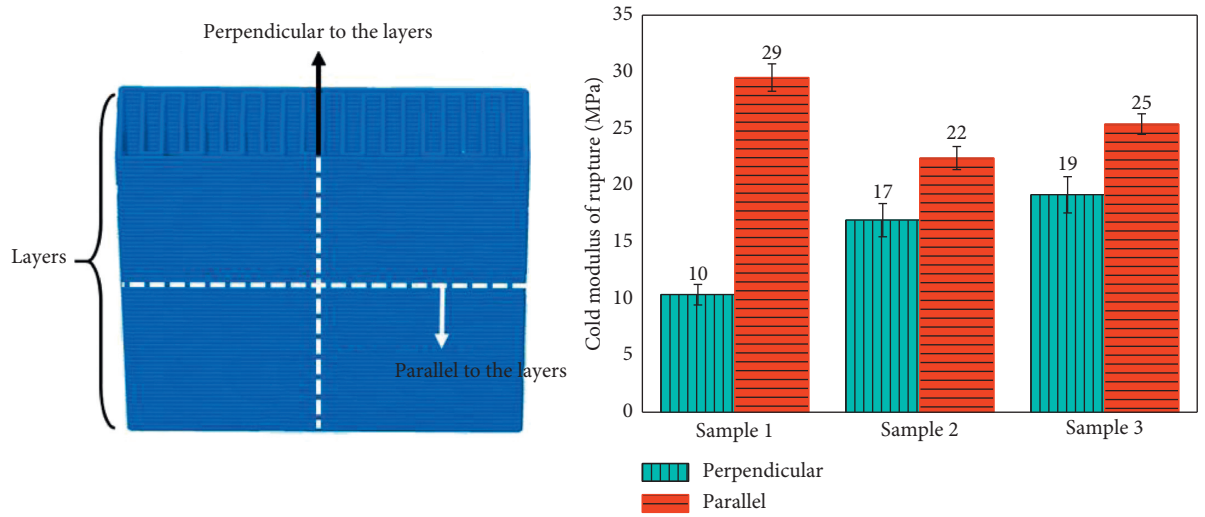

Figure 6: Cold modulus of rupture in different directions of samples: (1) vertical supporting structure, (2) oblique square grid supporting structure, and (3) honeycomb grid supporting structure.

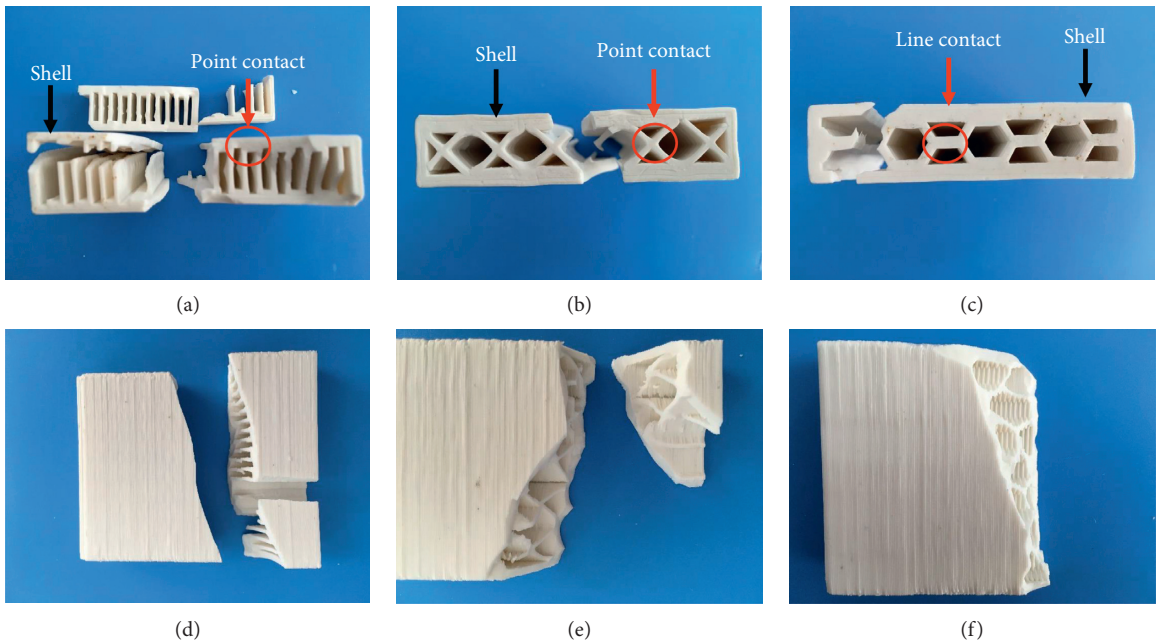

Figure 7: Failure modes in perpendicular direction and fracture surfaces of samples: (a) vertical supporting structure, (b) oblique square grid supporting structure, (c) honeycomb grid supporting structure in parallel direction, (d) vertical supporting structure, (e) oblique square grid supporting structure, and (f) honeycomb grid supporting structure.

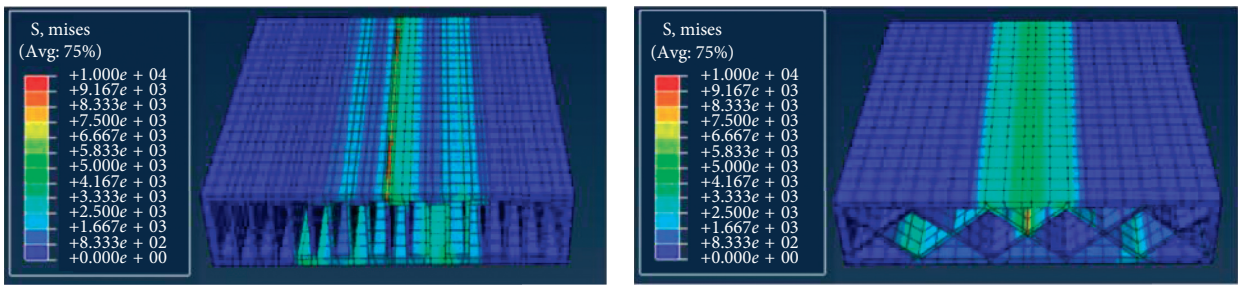

Figure 8: Continued.

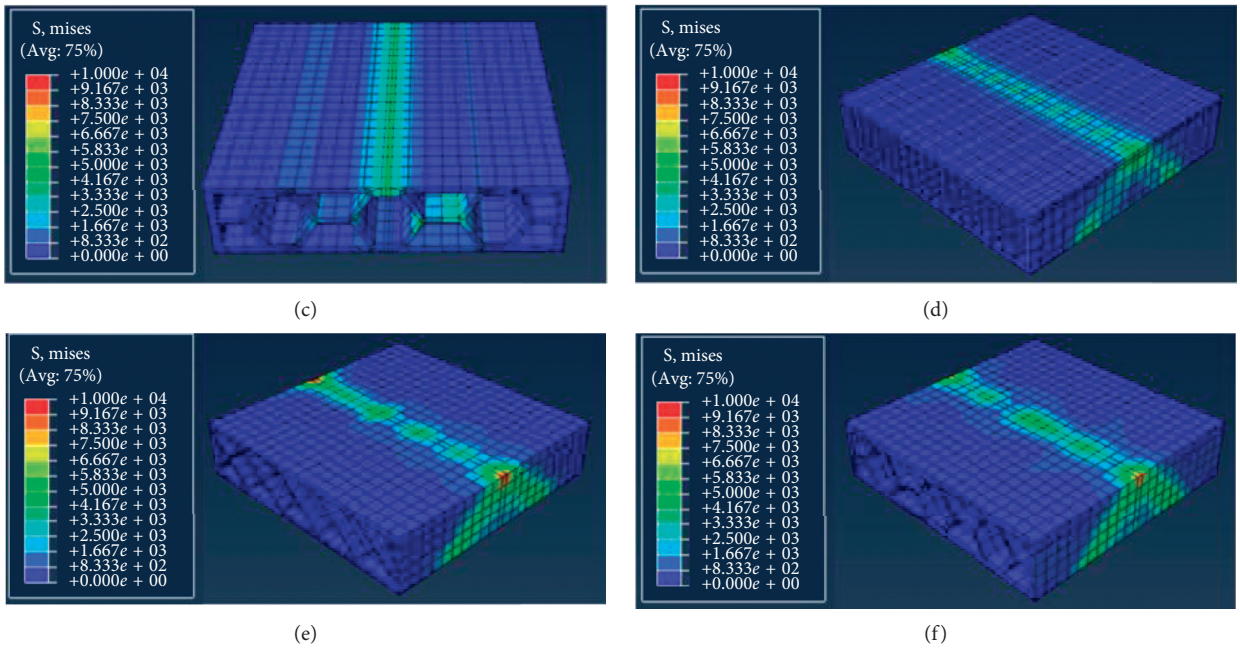

Figure 8: The stress components at integration points of three kinds of samples: (a) vertical supporting structure in perpendicular direction, (b) oblique square grid supporting structure in perpendicular direction, (c) honeycomb grid supporting structure in perpendicular direction, (d) vertical supporting structure in parallel direction, (e) oblique square grid supporting structure in parallel direction, and (f) honeycomb grid supporting structure in parallel direction.

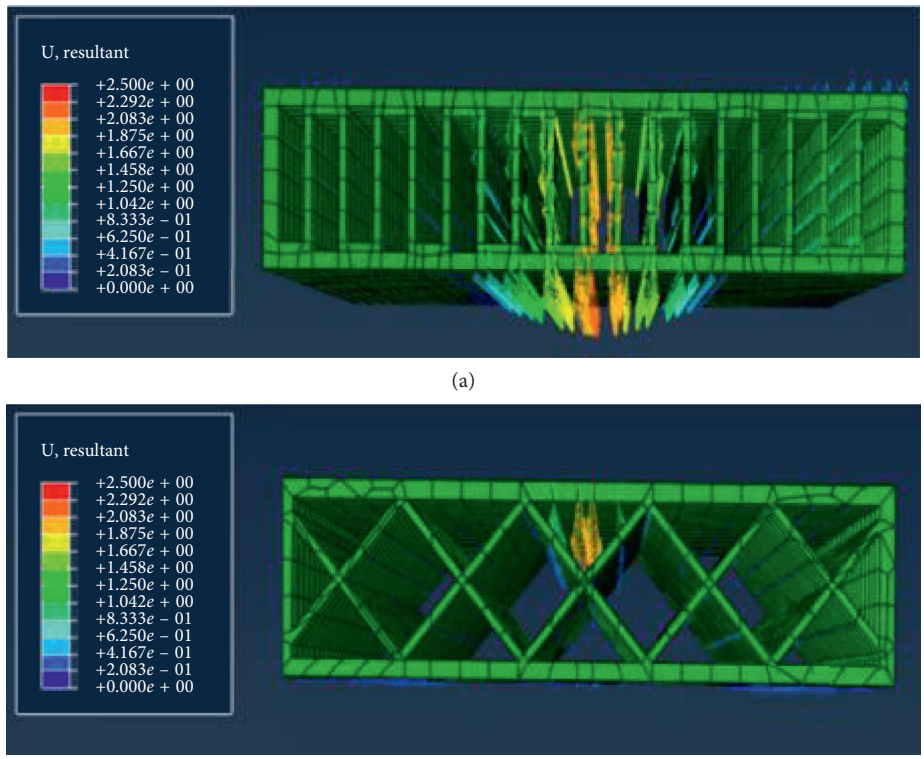

Figure 9: Continued.

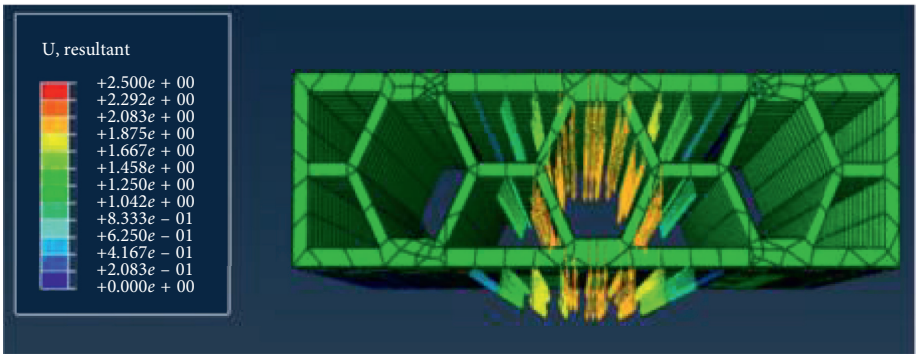

(c)

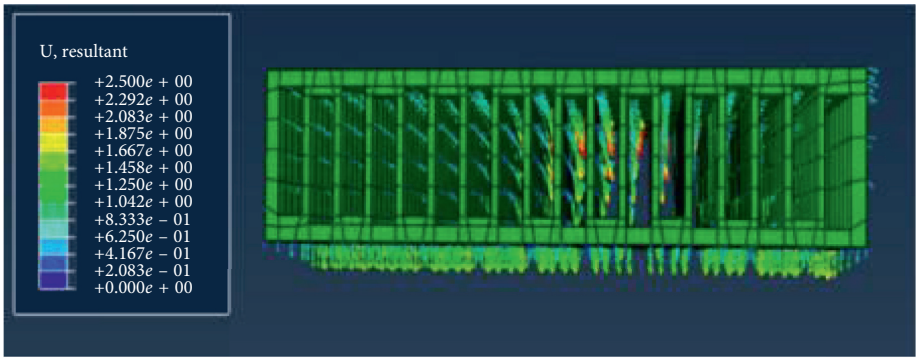

(d)

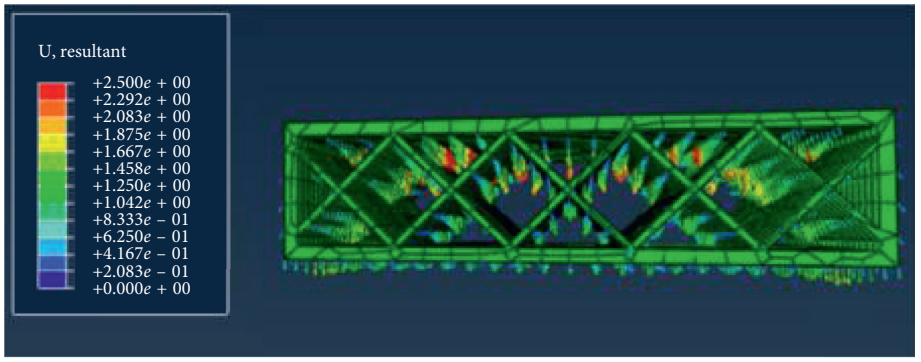

(e)

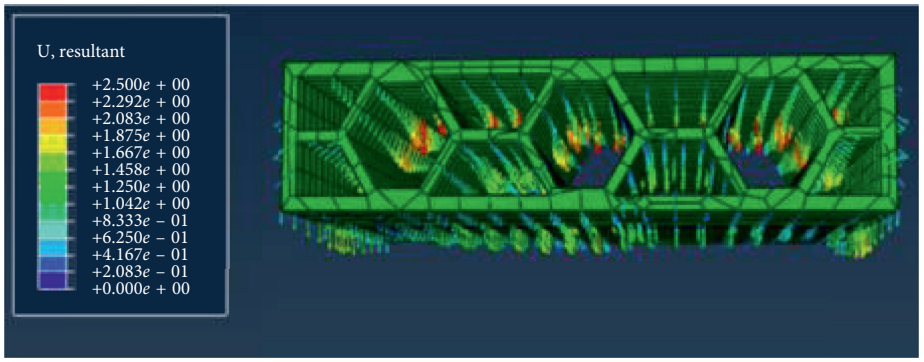

(f)

Figure 9: The tensile/compressive trend of three kinds of samples: (a) vertical supporting structure in perpendicular direction, (b) oblique square grid supporting structure in perpendicular direction, (c) honeycomb grid supporting structure in perpendicular direction, (d) vertical supporting structure in parallel direction, (e) oblique square grid supporting structure in parallel direction, and (f) honeycomb grid supporting structure in parallel direction.

4. Conclusions

For the first time, topological structure and 3D printing technology were used in the preparation of lightweight load bearing board. The present study emphasizes the importance of design of structures, because it has evident influence on the mechanical properties of 3D printed load bearing board. Results indicated that the mechanical properties of each sample are macro anisotropic. The results of validation concluded that when taking into account only structure the analysis of the cold modulus of rupture showed that honeycomb grid supported structure exhibited the highest strength in perpendicular direction and vertical supported structure exhibited the highest strength in parallel direction. Comparing with results obtained by three kinds of samples, honeycomb grid supported samples proved to be the most appropriate structure in various directions comprehensively. The finite element method (FEM) was applied and compared while modelling the mechanical properties based on the experimental findings. It could be inferred that under the perpendicular load distribution stress in the sample with vertical supporting structure was more nonuniform and the stress concentration was more evident by FEM. Compared with other load bearing boards, 3D printed load bearing board with honeycomb grid supported using kaolin as raw materials was more than 50% reduced in weight, and mechanical properties were enough for normal use.

Data Availability

The data used to support the findings of this study are available from the corresponding author upon request.

Conflicts of Interest

The authors declare that there are no conflicts of interest regarding the publication of this paper.

Acknowledgments

This work was supported financially by the National Natural Science Foundation of China (NSFC, Grant No. 51772139).

References

[1] C. Herrmann, W. Dewulf, M. Hauschild, A. Kaluza, S. Kara, and S. Skerlos, "Life cycle engineering of lightweight structures," *CIRP Annals*, vol. 67, no. 2, pp. 651–672, 2018.

[2] L. Fu, H. Gu, A. Huang, and H. Ni, "Correlations among processing parameters and porosity of a lightweight alumina," *Ceramics International*, vol. 44, no. 12, pp. 14076–14081, 2018.

[3] H. Yin, Y. Xin, J. Dang, K. Gao, Y. Tang, and H. Yuan, "Preparation and property of lightweight corundum-spinel refractory with density gradient," *Ceramics International*, vol. 44, no. 16, pp. 20748–20483, 2018.

[4] D. E. Njeumen Nkayem, J. A. Mbey, D. B. B. Kenne, and D. Njopwouo, "Preliminary study on the use of corn cob as pore forming agent in lightweight clay bricks: physical and mechanical features," *Journal of Building Engineering*, vol. 5, pp. 254–259, 2016.

[5] Z. Chen, Z. Li, J. Li et al., "3D printing of ceramics: a review," *Journal of the European Ceramic Society*, vol. 39, no. 4, pp. 661–687, 2018.

[6] L. Yeong-Jae, L. Kwang-Hee, and L. Chul-Hee, "Friction property of 3D printed ball bearing: feasibility study," *Results in Physics*, vol. 363, pp. 337–348, 2018.

[7] Z. C. Eckel, C. Zhou, J. H. Martin, A. J. Jacobsen, W. B. Carter, and T. A. Schaedler, "Additive manufacturing of polymer-derived ceramics," *Science*, vol. 351, no. 6268, pp. 58–62, 2016.

[8] P. Aditi, C. J. Leen, and K. Simon, "Scalability of 3D printed structured porous milli-scale reactors," *Chemical Engineering Journal*, vol. 363, pp. 337–348, 2019.

[9] B. Panda, M. Leite, B. B. Biswal, X. Niu, and A. Garg, "Experimental and numerical modelling of mechanical properties of 3D printed honeycomb structures," *Measurement*, vol. 116, pp. 495–506, 2018.

[10] T. Galeta, P. Raos, J. Stojšić, and I. Pakši, "Influence of structure on mechanical properties of 3D printed objects," *Procedia Engineering*, vol. 149, pp. 100–104, 2016.

[11] S. F. S. Shirazi, S. Gharehkhani, M. Mehrali et al., "A review on powder-based additive manufacturing for tissue engineering: selective laser sintering and inkjet 3D printing," *Science and Technology of Advanced Materials*, vol. 16, no. 3, pp. 1–20, 2015.

[12] L. Dong, "Mechanical responses of Ti-6Al-4V cuboctahedral truss lattice structures," *Composite Structures*, vol. 235, no. 1, Article ID 111815, 2020.

[13] X. Q. Zhou, L. Wang, D. Y. Yu, and C. Y. Zhang, "Dynamic effective equivalent stiffness analysis on the periodical honeycomb reinforced composite laminated structure filled with viscoelastic damping material," *Composite Structures*, vol. 193, no. 1, pp. 306–320, 2018.

[14] H. Rezaie, W. M. Rainforth, and W. E. Lee, "Mullite evolution in ceramics derived from kaolinite, kaolinite with added α-alumina and sol–gel precursors," *British Ceramic Transactions*, vol. 96, no. 5, pp. 181–187, 1997.

[15] C.-H. H. Hsiung, A. J. Pyzik, F. De Carlo, X. Xiao, S. R. Stock, and K. T. Faber, "Microstructure and mechanical properties of acicular mullite," *Journal of the European Ceramic Society*, vol. 33, no. 3, pp. 503–513, 2013.

[16] W. E. Lee, G. P. Souza, C. J. McConville, T. Tarvornpanich, and Y. Iqbal, "Mullite formation in clays and clay-derived vitreous ceramics," *Journal of the European Ceramic Society*, vol. 28, no. 2, pp. 465–471, 2008.

[17] S. P. K. Kohobhange, C. H. Manoratne, H. M. T. G. A. Pitawala, and R. M. G. Rajapakse, "The composition, unit cell parameters and microstructure of quartz during phase transformation from α to β as examined by in-situ high-temperature X-ray powder diffraction," *Journal of Physics and Chemistry of Solids*, vol. 117, pp. 131–138, 2018.

[18] A.-N. Chen, M. Li, J.-M. Wu et al., "Enhancement mechanism of mechanical performance of highly porous mullite ceramics with bimodal pore structures prepared by selective laser sintering," *Journal of Alloys and Compounds*, vol. 776, pp. 486–494, 2019.

[19] P. Li, Y. B. Guo, M. W. Zhou, and V. P. W. Shim, "Response of anisotropic polyurethane foam to compression at different loading angles and strain rates," *International Journal of Impact Engineering*, vol. 127, pp. 154–168, 2019.